A Graphical User Interface for Modeling the Optical Properties of Coated Metal Nanoparticles

H. A. Elmikaty [a], A. S. Samra [b], B. B. Yousif [c*]

[a,b] Electronics and Communications Dept., Faculty of Engineering- Mansoura University-Egypt
[c] Electrical and Communications Dept.- Faculty of Engineering-. -Kafrelsheikh University- Egypt

Abstract
This paper presents a graphical user interface, based on modified long-wavelength approximation method (MLWA) to compute the optical properties of core-shell nanoparticles. The validity of this technique is verified by comparison to the exact solution (Mie theory). For core-shell nanoparticles, when the shell thickness of a core-shell particle is decreased, the plasmon resonance shifts to longer wavelengths. This red shift is accompanied by an increase in peak intensity. For coated spherical particles, we confirm that our approach yields a correspondence with Mie theory and gives an approximation error of less than 2.8% for silica-gold and silica-silver particles with outer diameters approaching 40nm and 26nm and inner diameters approaching 38nm and 24nm respectively. Also the MLWA can give an acceptable degree of accuracy 4.92% for larger particles of silica-gold with (inner-outer) diameters 68-70nm at surface plasmon resonance wavelength 1573nm. For this simulation run, the computation time was less than 150.050 ms (Intel Pentium 4 CPU at 3GHz, 1.00GB of RAM), which includes calculation of the polarizability and all three cross-section plots of absorption, scattering and extinction. This simulator provides a useful guide tool for optical characterization experiments.

Keywords:
optical properties; coated nanoparticles; surface plasmon resonance, numerical simulation

1. Introduction

Metal nanoshells are a novel type of composite spherical nanoparticle consisting of a dielectric core covered by a thin metallic shell. These particles are often composed of coinage metals such as copper, silver, or gold. When excited with an electromagnetic field, nanoparticles produce an intense absorption attributed to the collective oscillation of electrons on the particle surface, termed a surface plasmon resonance (SPR). The resonant frequency is highly dependent on particle size, shape, material, and environment[1-3]. By varying the relative dimensions of core and shell, the optical resonance of these nanoparticles can be precisely and systematically varied over a broad region ranging from the near-UV to the mid-infrared. These making nanoparticles attractive as functional materials for many applications. Some examples include electronic and optical devices[4] chemical and biological sensors[5], optical energy transport[6], high-density optical storage platforms [7], Biomedical Applications[8-9], Spheroidal nanoparticles as nanoantennas for fluorescence enhancement[10], Applications of gold nanoparticles in cancer nanotechnology and Tumour Therapy[11], thermal ablution.[12], Spectral imaging [13] and Solar applications[14].

Experimentalists have been able to synthesize uniform colloidal particles for sometime. New experimental techniques have recently produced core/shell nanoparticles with a consistent size and shape[15]. A strong plasmon resonance is observed when the layered particle is composed of silica and gold, which can be shifted by adjusting the relative thickness of the core and shell material. The concentric sphere geometry of the particles allows for control of optical properties in a highly predictive manner, making them a new class of materials that are capable of tailoring radiation throughout the visible and infrared wavelength regimes[16-17]. The fundamental optical properties of individual and multiple metal nanoparticles can be difficult to discern experimentally [18]. Therefore, a simple and user-friendly simulation platform to help guide experiments would be useful.

For the purpose of gaining insight and basic quantitative information about the linear optical properties of ellipsoidal nanoparticles, numerical methods are computationally time consuming and complex[19]. However, in focusing our attention on particles which are much smaller compared to the wavelength of light, a simpler solution to the non-spherical scattering problem presents itself in the form of an electrostatics treatment, recently termed, the modified long-wavelength approximation (MLWA) [20].

The outline of the paper is as follows. Section 2 introduces a brief review of modified long-wavelength approximation method to compute the scattering, absorption, and extinction for homogenous and coated spheroidal metal nanoparticles. Section 3 explains the underlying theory used in our simulations and discuss GUI functionality with some examples of completed simulations runs. Section 4 analyzes the accuracy of the approximations and the effects of the optical constants source data. Finally, we summarize our observations and discuss potential future extensions of the GUI.

Manuscript received March 5, 2011
Manuscript revised March 20, 2011

2. Modified long-wavelength method

The MLWA is an extension of the basic quasi-static approximation and its derivation can be found in [21]. The GUI developed here uses the MLWA to calculate the optical properties of both spherical and non-spherical coated nanoparticles.

The polarizability using the standard quasi-static approximation [22] as

$$\alpha_\beta(w) = \frac{(\frac{4\pi abc}{3})(\varepsilon_1(w) - \varepsilon_m)}{\varepsilon_m + (\varepsilon_1(w) - \varepsilon_m)L_\beta} \qquad (1)$$

for spheroid with major and minor radii, a and b, in a non-absorbing, homogeneous surrounding medium with dielectric constant, εm. where β= a, b, c and Lβ is a depolarization factor[23] calculated for each of the three principal axes that accounts for shape effects. For spheres, a= b= c, prolate spheroids, a > b=c and oblate spheroids, a=b > c. The particle is assumed to be oriented with its center at the origin, its major axis parallel to the x-axis, and the incident light traveling along the +z direction. The polarizability of coated ellipsoid is given by Eq. (2)[3].

$$\alpha_\beta(w) = \frac{v(\varepsilon_2 - \varepsilon_m)[\varepsilon_2 + (\varepsilon_1 - \varepsilon_2)(L^1_\beta - fL^2_\beta)] + f\varepsilon_2(\varepsilon_1 - \varepsilon_2))}{([\varepsilon_2 + (\varepsilon_1 - \varepsilon_2)(L^1_\beta - fL^2_\beta)][\varepsilon_m + (\varepsilon_2 - \varepsilon_m)L^2_\beta] + fL^2_\beta\varepsilon_2(\varepsilon_1 - \varepsilon_2))} \qquad (2)$$

where $v=4\Pi a_2b_2c_2/3$ is the volume of the particle, $f= a_1b_1c_1 / a_2b_2c_2$ is the fraction of the total particle volume occupied by the inner ellipsoid, L^1_β and L^2_β are the geometrical factors for the inner and outer ellipsoids given in [3], ε_1 is permittivity of the core (inner) ellipsoid with semiaxes a_1, b_1, c_1 and ε_2 is permittivity of the shell (outer) ellipsoid with semiaxes a_2, b_2, c_2. The theory of MLWA is described as follows. To account for dynamic depolarization and radiative damping effects, we introduce two correction terms to the polarizability in Eq. (1,2) such that[20]

$$\tilde{\alpha}_\beta(w) = \frac{\alpha_\beta(w)}{\underbrace{1 - \frac{k^2}{4\pi\beta}\alpha_\beta(w)}_{\text{dynamic depolarization}} \underbrace{- i\frac{k^3}{6\pi}\alpha_\beta(w)}_{\text{radiative damping}}} \qquad (3)$$

where $k=2\Pi(\varepsilon_m)^{0.5}/\lambda$. It is this corrected form of the quasi-static approximation that permits the calculation of the absorption, scattering, and extinction cross-sections of single particles with major-axes up to 10% of the incident wavelength [24]. The extinction cross-section is the sum of the scattering and absorption cross-sections given by

$$C_{sca} = \frac{k^4}{6\pi}\left|(\xi_1\tilde{\alpha}_1 + \xi_2\tilde{\alpha}_2)\right|^2 \qquad (4)$$

$$C_{abs} = k\,\mathrm{Im}[\xi_1\tilde{\alpha}_1 + \xi_2\tilde{\alpha}_2] \qquad (5)$$

respectively, where $\xi_1=1$ and $\xi_2=1$ correspond to incident light polarization along the *x* and *y* directions, respectively. For 45° polarized light, $\xi_1= \xi_2 =0.5$.

3. Graphical user interface (GUI)

A GUI is developed using MATLAB's to calculate the scattering, absorption and extinction cross-sections and efficiencies for homogenous and coated spheroidal metal nanoparticles due to an incident *x* or *y* or *45°*-polarized and z-traveling plane wave. Optical constants data for gold, silver, and copper[25-26] are included with the GUI along the dielectric constants for oil, vacuum and water. However, user-specified values for other materials and media can also be entered. Also, user can choose the wavelength or energy and the polarization of the incident light.

In the case of coated spheroids the core permittivity ε_1 can be entered with any value of non-absorbing material. The plotting options for the GUI are for a given particle of interest: the complex dielectric function, the complex polarizability and the absorption, scattering, extinction cross-sections/efficiencies. The GUI includes a functions to compare the results of a spherical particle with those calculated using Mie theory and determine the SPR location and amplitude. In all cases, the results of these plots can be plotted against incident wavelength. The wavelength range of the computed spectra (188 nm- 1942 nm) and depends entirely on that of the source used for the optical constants data.

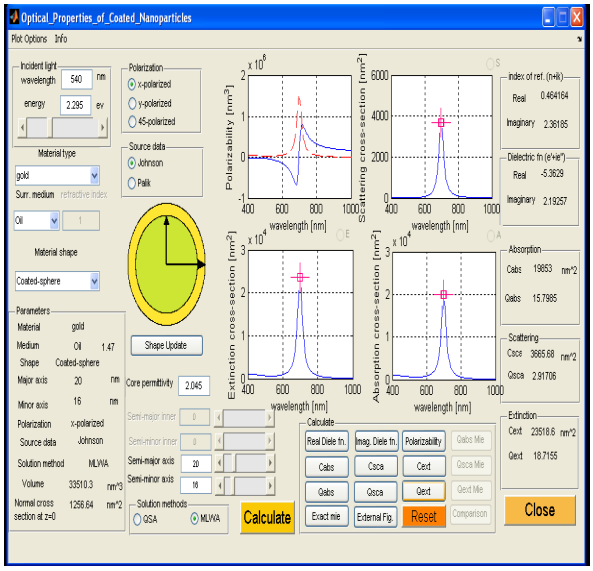

Fig. 1. A screen shot of the GUI after a completed simulation run for a silica/gold (core/shell) sphere (shell radius=20 nm, core radius=16 nm),in oil (εm=2.16), with source data[25] and x-polarized light.

Fig. 1. shows a screen shot of the GUI after a completed simulation run for a silica/gold (core/shell) sphere (shell radius=20 nm, core radius=16 nm), in oil (εm=2.16), with source data[25] and x-polarized light.

The values in the output panels at the right are for an incident wavelength of 540nm, the plasmon resonance shifts to longer wavelengths at 698 nm. Here only the polarizability, absorption, scattering, and extinction cross-sections are shown.

Fig. 2 indicates a difference between homogenous gold sphere and silica/gold sphere at the same diameter 40 nm, in oil medium, with source data[25] and 45o-polarized light using MLWA method. It is obvious that there is a large difference in plasmon resonance wavelength (540nm /698 nm) and the peak (5.2/18.8) at shell thickness 4 nm of an extinction efficiency. A strong plasmon resonance is observed when the layered particle is composed of silica and gold, which can be shifted by adjusting the relative thickness of the core and shell material. The concentric sphere geometry of the particles allows for control of optical properties in a highly predictive manner, making them a new class of materials that are capable of tailoring radiation throughout the visible and infrared wavelength regimes. This clear the advantage of silica/gold sphere over a homogenous gold sphere.

Fig. 3 differentiates between homogenous silver prolate and silica/silver prolate at the same outer aspect ratio η0=2, for a major axis 4 nm in water medium, with source data[25] and x- polarized light

using MLWA method. It is clear that there is a large

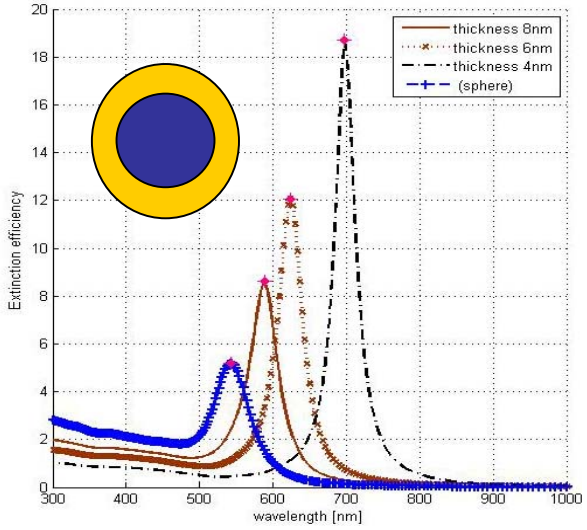

Fig. 2 shows a difference between homogenous gold sphere and silica/gold sphere at the same diameter 40 nm, in oil medium, with source data[25] and 45o-polarized light using MLWA method.

difference in plasmon resonance wavelength (477 nm /660 nm) and the peak (6/5.9) at inner aspect ratio η_i =2.33 of an extinction efficiency. Also as the same in coated gold sphere, a strong plasmon resonance is observed when the layered particle is composed of silica and silver, which can be shifted by adjusting the relative thickness of the core and shell material.

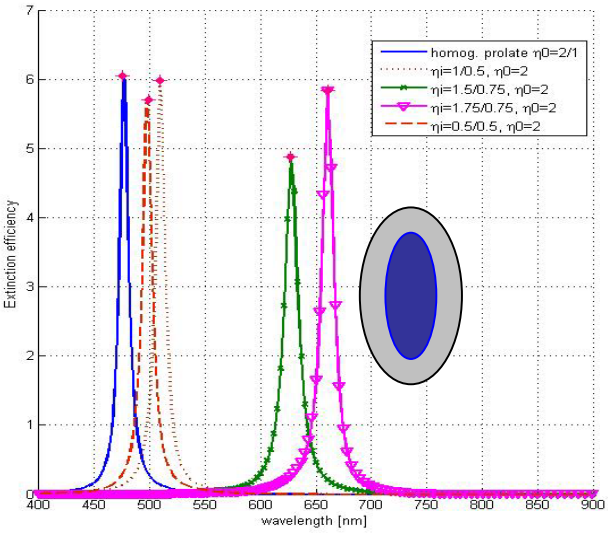

Fig. 3 shows a comparison between homogenous silver prolate and silica/silver prolate at the same outer aspect ratio (η0=2) with major axis 4 nm in water medium, and varying inner aspect ratio ηi

Extinction efficiency of a gold oblate spheroids (a=b >c) and silica/gold oblate at the same outer aspect ratio η_0=2, for a major axis 12.6 nm in vacuum medium, with source data[26] and 45^o-polarized incident light using MLWA is shown in Fig. 4. We note that when the shell thickness is decreased the large plasmon resonance in position and peak is observed.

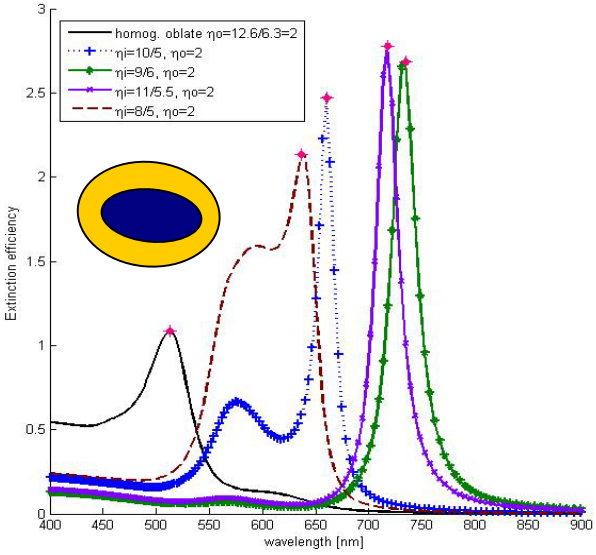

Fig. 4 shows a comparison between homogenous gold oblate spheroids(a=b >c) and silica/gold oblate at the same outer aspect ratio η0=2.

4. Validity of the MLWA and effect of optical constants source data

In general, the limiting factor of the MLWA is its accuracy for larger particles. In its formal derivation, the MLWA may only be applied to particles with sizes that are 10% of the incident wavelength [24]. However, the MLWA can give an acceptable degree of accuracy for larger particles as we show here.

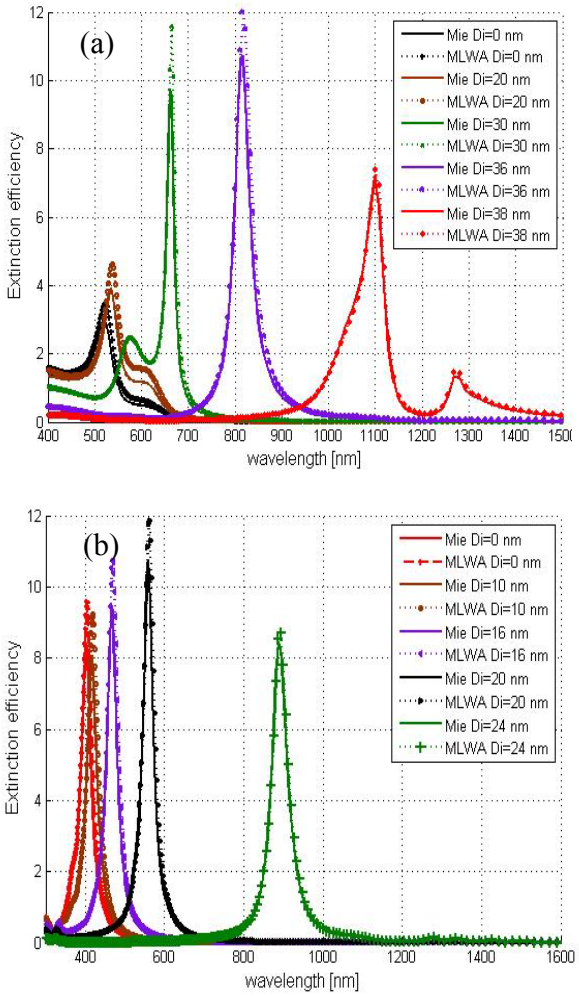

Fig. 5. Comparison of extinction spectra calculated

using the MLWA and Mie theory (solid lines) for various inner diameter of (a)silica-gold sphere with fixed outer diameter of gold at 40nm and (b) silica-silver sphere with fixed outer diameter of silver at 26 nm in water with x-polarized and source data[26].

The GUI includes a comparison pushbutton to quickly gauge the accuracy of results for spherical particles by comparing them against those obtained using Mie theory.

Fig. 5 shows calculated extinction efficiencies using Mie theory(solid lines) and the MLWA(dashed lines) for various thickness of silica-gold in Fig. 5a and silica-silver in Fig. 5b. We observe a correspondence between the two models for particles that are 38- 40 nm(inner- outer) diameters of the silica-gold particles and 24-26 nm (inner-outer) diameters of the silica-silver particles and gives an approximation error of less than 2.8% when comparing the SPR peaks obtained using Mie theory and the MLWA. For a given silica-gold or silica-silver particle with fixed outer diameter and increasing the inner diameter of silica as shown in Fig. 5 the plasmon resonance shifts to longer wavelengths. This red shift is accompanied by an increase in peak intensity and this very useful in many applications. By varying the relative dimensions of core the SPR percent error minimized from 15% at core radius zero (homogenous gold sphere with diameter 40 nm) to 2.8% at core radius 38 nm (silica-gold sphere with diameters 38- 40 nm).

As similar degree of error occurs for a silica-silver particle of 26 nm outer diameter and 24 nm inner diameter (Di) of silica core as in Fig. 5b. These results are summarized in tables (1,2). We observe that when the shell thickness of a core/shell particle is decreased, the plasmon resonance shifts to longer wavelengths and the SPR percent error is minimized.

Table 1: SPR Percent error of silica/gold sphere

Di nm	MLWA		Mie theory		SPR error %	
	λ	Mag.	λ	Mag.	Mag.	Pos.
0	402	9.56	401	8.48	13.2	0.25
10	419	9.2	415	8.12	13.3	0.96
16	471	10.72	469	9.49	12.96	0.42
20	561	11.84	559	10.86	9.02	0.36
24	893	8.7	888	8.47	2.72	0.71

Table 2: SPR Percent error of silica/silver sphere

Di nm	MLWA		Mie theory		SPR error %	
	λ	Mag.	λ	Mag.	Mag.	Pos.
0	519	3.46	521	2.99	15.72	0.38
20	537	4.63	535	3.94	17.51	0.37
30	665	11.56	661	9.75	18.56	0.61
36	817	11.95	817	10.79	10.75	0
38	1100	7.38	1100	7.19	2.78	0

Fig. 6 demonstrates the size dependence of the MLWA for silica/gold spheres. Clearly, the MLWA can give an acceptable degree of accuracy for larger particles as obviously in table (3). When the silica core diameter (Di) is 38 nm and varying the gold shell diameter (Do) from 40 to 60 nm the SPR percent error is increases, but at Di=68nm and Do=70nm, the SPR percent error is 4.92 % and the resonance wavelength is 1574nm. This is a very useful case in many applications.

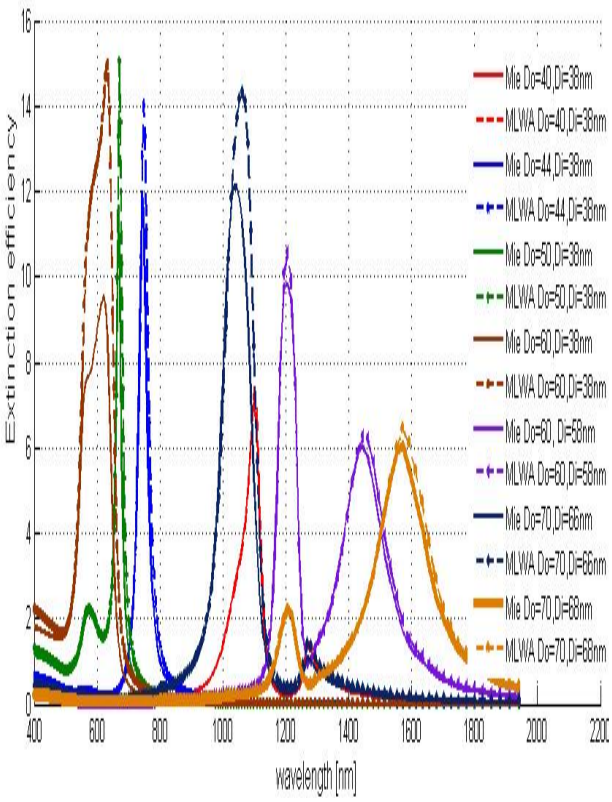

Fig. 6. Comparison of Mie theory (Solid lines), and MLWA (dash lines) for various particle sizes of silica-gold sphere in water medium, with x-polarized and source data[26].

Table 3: SPR Percent error of silica/gold sphere in water, when comparing the SPR peaks obtained using Mie theory and the MLWA.

Do nm	MLWA		Mie theory		SPR error %	
	λ	Mag.	λ	Mag.	Mag.	Pos
40	1100	7.38	1100	7.19	2.78	0
44	751	14.06	748	11.99	17.27	0.6
50	672	15.04	668	11.68	28.78	0.54
60	630	14.99	620	9.58	57.05	2.03
70	1574	6.42	1569	6.1	4.92	0.32

The optical constants data that are input to the GUI are taken directly from experiments by Johnson and Christy [25] and Palik [26]. The modular nature of the GUI permits one to quickly compare the effects of different source data on the calculations. An example of this is shown in Fig. 9 In Fig. 9a, for a gold sphere (diameter 40 nm) in water, we observe appreciable differences in the spectra for wavelengths that are blue of the plasmon resonance peak. Alternatively, in Fig. 9b, for a silver sphere with the same diameter in water, the difference in spectra is more pronounced in the vicinity of the plasmon resonance. Therefore, this reiterates the fact that the source data should be considered when interpreting results.

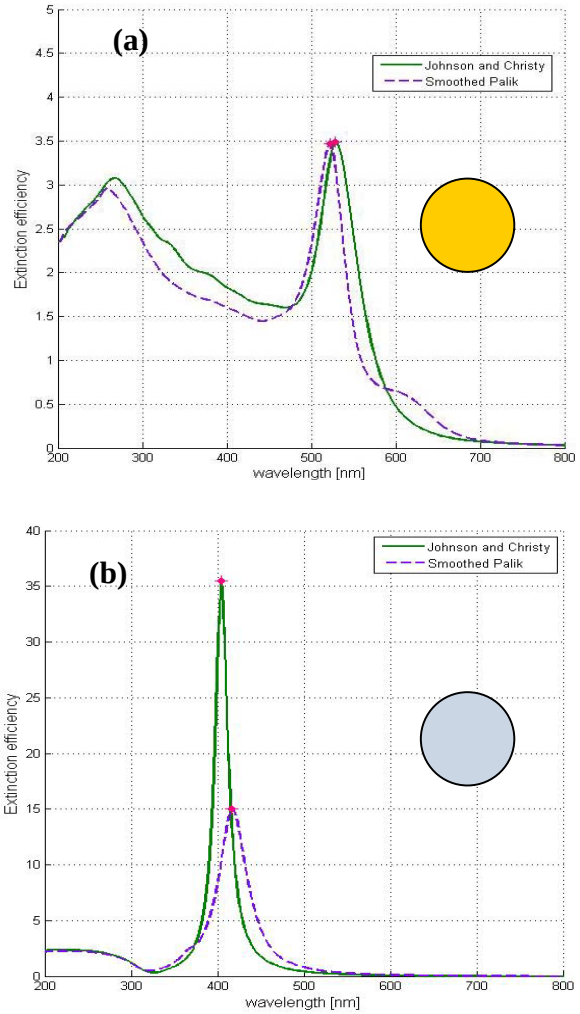

Fig. 7 Comparison of extinction spectra of 40-nm diameter spheres of (a) gold and (b) silver calculated using optical constant data from two different sources. Both figures show differences in SPR width and SPR peak magnitude

5. Conclusion

An interactive GUI based on MLWA is developed to calculate and display the absorption, scattering, and extinction fields of a homogenous and coated spheroidal nanoparticles. The accuracy of the MLWA to ellipsoidal particles was analyzed in comparison to Mie theory. It was found that, in general, the accuracy of the MLWA decreases as the particle volume increases, but gives an approximation with less than 2.8% error for silica/gold nanoparticle with silica (core) diameter of 38 nm and gold (shell) diameter of 40 nm. Also the same error result obtained for silica/silver nanoparticle with diameters approaching 24-26 nm (core-shell). A Core/shell nanoparticles display a red shift and an increase in intensity

of extinction by varying the relative dimensions of the core and the shell, the optical resonance of these nanoparticles can be precisely and systematically varied over a broad region ranging from the near-UV to the mid-infrared. So nanoshells possess highly favorable optical and chemical properties for biomedical imaging and therapeutic applications. In addition to spectral tunability, nanoshells offer other advantages over the homogenous spheres including improved optical properties and minimized the SPR percent error from 15% to 2.8%.

We also discussed the effects of different source data for the optical constants and found that it can be appreciable, which must be considered when interpreting the output of such simulations. In summary, the simulation platform provides many functions to gain insight and generate qualitative information about the linear optical properties of metal nanoparticles. Moreover, the speed and accuracy of computation makes it a convenient alternative to those that employ exact numerical methods, particularly when investigating nonspherical particles. Further studies are in progress to apply the simulation tool to investigate multilayer and multiple particles.

References

[1] E. Kooij, B. Poelsema, "Shape and size effects in the optical properties of metallic nanorods", J Chem Phys, 8, 3349–57(2006).

[2] U.Kreibig, M. Vollmer, "Optical properties of metal clusters", 1st ed., Berlin, Springer, 1995.

[3] C. Bohren, D. Huffman, "Absorption and scattering of light by small particles", Weinheim: Wiley-VCH; 1983.

[4] Y. Dirix, C. Caseri and Smith, et al.," Oriented pearl-necklace arrays of metallic nanoparticles in polymers: a new route toward polarization-dependent color filters", J Adv Mater, 11, 223–227(1999)

[5] C. Loo, ,L. Lin, A. Hirsch, M. Lee, J. Barton, Halas N, et al.," Nanoshell enabled photonics-based imaging and therapy of Cancer", J Tech. Canc. Resrch. Trmnt, 3, 33–40(2004).

[6] H. J. Lezec, A. Degiron, , E . Devaux, R.A. Linke, L . Martin-Moreno., F.J Garcia-Vidal, and T.W. Ebbesen, "Beaming light from subwavelength aperture", Sciencemag.org, 297, 820-822(2002).

[7] C. JWM, C. Bullen, P. Zijlstra, "Spectral encoding on gold nanorods doped in a silica sol–gel matrix and its application to high-density optical data storage", J Adva Mater, 17, 875–80(2007).

[8] A. T. Erickson and J. W. Tunnell "Gold Nanoshells in Biomedical Applications, Nanomaterials for the Life Sciences , Mixed Metal Nanomaterials", Edited by Challa S. S. R. Kumar, 3, 1-44(2009).

[9] H. Xiaohua, N. Svetlana, and M. A. Elsayed, "Gold Nanorods: From Synthesis and Properties to Biological and Biomedical Applications", J Adva Mater, 21, 4880–4910(2009).

[10] A. Mohammadi, F. Kaminski, V. Sandoghdar and M. Agio, "Spheroidal nanoparticles as nanoantennas for fluorescence enhancement", Int. J. Nanotechnol., 6, 902-914(2009).

[11] M. Geoffrey , P. Ji-Ho, A. Amit, K. Nanda, K. Das, J. Michael, and N. Sangeeta, "Computationally Guided Photothermal Tumor Therapy Using Long-Circulating Gold Nanorods Antennas", www.aacrjournals.org, Cancer Res, 69, 1-9(2009).

[12] Hirsch, Stafford, Bankson, et al., "Nanoshell mediated near-infrared thermal therapy of tumors under magnetic resonance guidance", Proc Nat Acad Sci (PNAS), 100: 13549–13554(2003).

[13] L. J. Steven, S. Ravikant and C. Niloy, "Rapid spectral analysis for spectral imaging", J OSA, 1:157-164(2010).

[14] S. Pillai, , et al., " Enhanced Emission from Si-Based Light-Emitting Diodes Using Surface Plasmons", J Appl phys Letters, 88, 161102(2006).

[15] Y. Ken-Tye, S. Yudhisthira, T. S Mark, N. P. Paras , "Synthesis and plasmonic properties of silver and gold nanoshells on polystyrene cores of different size and of gold–silver core–shell nanostructures", J Colloids and Surf A, 290, 89–105(2006).

[16] S. J. Oldenburg, Averitt, S. L. Westcott and et al., "Nanoengineering of Optical Resonances", J Chem Phys, 288, 243–247(1998).

[17] S. J. Oldenburg,, S. L. Westcott, , R. D. Averitt and et al., " Surface enhanced Raman scattering in the near infrared using metal nanoshell substrates ", J Chem. Phys. 111: 4729–4735(1999).

[18] M. Mishchenko, L. Travis, A. Lacis , "Scattering, absorption, and emission of light by small particles", 1st ed New York, 2004.

[19] P.W. Barber, R.K. Chang, H. Massoudi , "Electrodynamic calculations of the surface- enhanced electric intensities on large Ag spheroids", Phys Rev B27,7251–61(1983).

[20] Y . Wen-Hui, G. C. Schatz, V. Duyne, "Discrete dipole approximation for calculating extinction and Raman intensities for small particles with arbitrary shapes", J Chem Phys, 103, 869–75(1995).

[21] M . Meier and A. Wokaun, "Enhanced fields on large metal nanoparticles: dynamic depolarization", Opt Lett,8,581–3(1983).

[22] D. Kaspar , C. Kimani, J. Toussaint , "A simple GUI for modeling the optical properties of single metal nanoparticles", JQSRT, 110, 1037– 1043(2009).

[23] J. Osborn, "Demagnetizing factors of the general ellipsoid", J Phys Rev, 67, 351–357(1945).

[24] T. R. Jensen , L. Kelly, A. Lazarides, and G. C. Schatz, "Electrodynamics of Noble Metal Nanoparticles and Nanoparticle Clusters", J Cluste Sci, 10, 295–317(1999).

[25] P.B. Johnson and R.W. Christy, " Optical constants of the noble metals" , Phys Rev B, 6, 4370–4379(1972).

[26] E. Palik , "Handbook of optical constants of solids", 1st ed, New York: Academic Press,1985.